Journal of Energy Storage 55 (2022) 105676

Contents lists available at ScienceDirect

Journal of Energy Storage

journal homepage: www.elsevier.com/locate/est

Research papers

Empirical calendar ageing model for electric vehicles and energy storage systems batteries

Gaizka Saldaña [a,*], José Ignacio San Martín [b], Inmaculada Zamora [a], Francisco Javier Asensio [b], Oier Oñederra [a], Mikel González-Pérez [b]

[a] Electrical Engineering Department, Engineering School of Bilbao, University of the Basque Country UPV-EHU, Bilbao 48013, Spain
[b] Electrical Engineering Department, Engineering School of Gipuzkoa (Section of Eibar), University of the Basque Country UPV-EHU, Eibar 20600, Spain

ARTICLE INFO

Keywords:
Calendar ageing
Lifetime model
Battery degradation
Lithium-ion battery
Electric vehicle

ABSTRACT

Transport electrification and energy storage are considered part of the solution to decrease CO_2 emissions from the energy and transport sectors. In this context, batteries can be a promising technology, since advances in the last few years have ensured a larger lifetime and better performance. Depending on actual use of the batteries, calendar ageing can be considered as the main origin of degradation in both transport electrification and energy storage since electric vehicles are parked 96 % of the time and battery energy storage stations (BESSs) can remain at a high State of Charge (SoC) for a long time along their lifetime. Therefore, a lifetime model or a degradation model of batteries is necessary to optimally develop an application of these in every sector. In this sense, this paper presents a calendar ageing model of a nickel-manganese-cobalt (NMC) battery, which is used in commercialised electric vehicles. The degradation model presented here is based on the Hermite Cubic Interpolation Polynomial (PCHIP) over an experimental results data set in combination with a power law for modeling the influence of the storing time. In this context, four fitting equations have been compared in search of the most appropriate time depending rate, and the accuracy of the most commonly used model was improved. The storing temperature and SoC have been found to be the most harmful factors in the degradation of these batteries by calendar ageing. The degradation model developed yields of an average root-mean-square error (RMSE) of 0.8 % in capacity fade (CF), while in power fade (PF), the average RMSE has been 2.3 %.

1. Introduction

Traditionally, lithium-ion batteries have been used in portable electronics and have only been required for a few years of their lifetime. However, electric vehicles are high specific energy and high specific power loads with the desired lifetime of 10–15 years while taking several climatic conditions into consideration. The state of health (SoH) of a battery can be checked in the maximum usable range of an electric vehicle (EV), but SoH also affects its residual value since the battery accounts for nearly 65 % of its total cost [1]. Consequently, a battery needs to be replaced because it reaches its end-of-life (EoL) when its capacity retention is below 80 %, compared to a fresh one [2].

Degradation in battery cells usually takes place due to a combination of cycle and calendar ageing. Cycle ageing is the degradation given by the use or the cycle of the cell, and it is related to the charge and discharge current with respect to its nominal capacity (C-Rate), Depth of Discharge (DoD), number of cycles performed (N) and temperature (T). Charging mode has a great relevance in cycle ageing, affected by fast charging or charging at extreme temperatures, among others. However, calendar ageing is related to the degradation of the cell independent of charge-discharge, and it is related to the storing average State of Charge (SoC), time (t) and temperature of storing (T). Some of the studies on calendar ageing modeling are presented later in this section.

Although it is very expensive, it is possible to test the cycle ageing process of a battery along its entire lifetime; however, testing for calendar ageing is time intensive and usually only considers a few ageing

Abbreviations: BESS, battery energy storage stations; BMS, battery management systems; CF, capacity fade; C-Rate, current-rate; DoD, depth-of-discharge; EoL, end-of-life; EV, electric vehicle; HEV, hybrid electric vehicle; LFP, lithium-iron-phosphate; LLI, loss of lithium inventory; N, number of cycles; NCA, nickel-cobalt-aluminium; NMC, nickel-manganese-cobalt; PCHIP, Hermite Cubic Interpolation Polynomial; PF, power fade; R^2, correlating factor; RMSE, root-mean-square error; SEI, solid electrolyte interphase; SOC, state of charge; SoH, state of health; T, Temperature; t, time.

* Corresponding author.
E-mail address: gaizka.saldana@ehu.eus (G. Saldaña).

https://doi.org/10.1016/j.est.2022.105676
Received 12 January 2021; Received in revised form 11 September 2022; Accepted 13 September 2022
Available online 22 September 2022

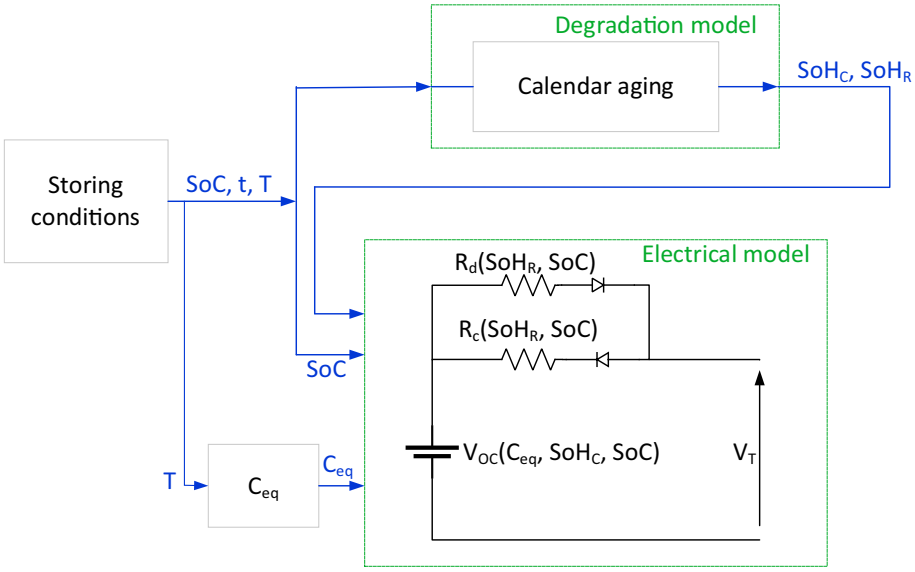

Fig. 1. Structure of the developed model.

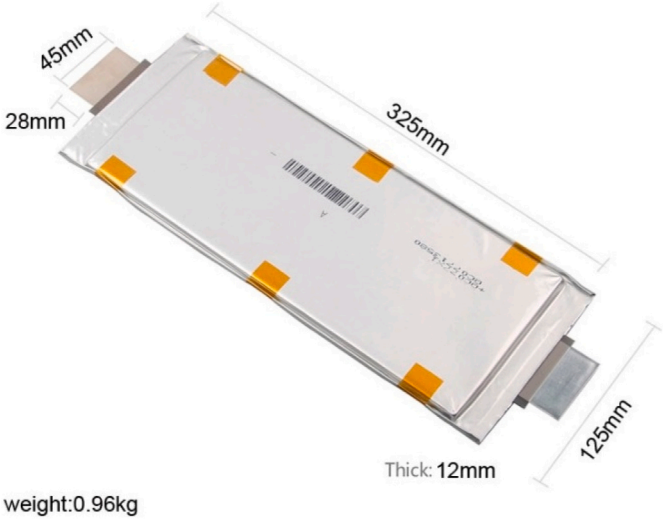

Fig. 2. Studied cell: LG E63.

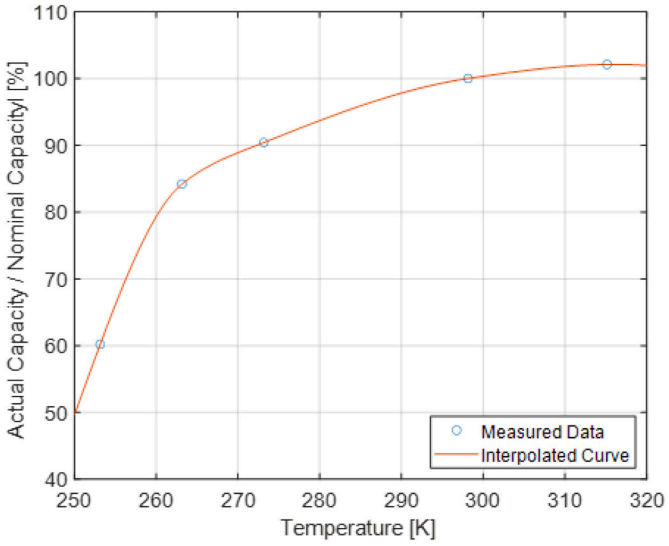

Fig. 3. Useful capacity–temperature graph.

Table 1
Basic data about the LG E63 cell.

Discharge capacity	25 °C, 2.50–4.20 V Standard charge/discharge 21.6 A	Nominal: 65.6 Ah Minimum: 64.6 Ah
	25 °C, 2.50–4.20 V Standard charge/discharge 32.5 A	Nominal: 64.8 Ah Minimum: 63.8 Ah
Nominal voltage		3.60 V
Voltage		2.50–4.20 V
Continuous operation temperature		10 °C–45 °C

conditions [3,4]. Furthermore, the development of degradation models is justified, as a vehicle remains parked for approximately 96 % of the time [3,5–7] and Battery Energy Storage Stations (BESSs) can spend a significant amount of time, i.e. around 10 % of their lifetime, out of operation [8]. In the case of BESS, its state is defined by intervals (charging, discharging and not operating); the range of the operating SoC is limited to that set when designing it [9], and an attempt is made to avoid dwell time at high SoC [10]. Furthermore, risky situations such as large and fast variations of charge and discharge rates as well as depths of discharge must be avoided [11,12], while further research is being developed in this thermal runaway topic [13–16]. This is the reason why calendar ageing models are of great use in electromobility and energy storage while modernising the electric grid [3,17,18].

The degradation of a battery is a normal process that permanently decreases the amount of energy that a battery can store as well as the amount of power it can supply. The degradation mechanisms that are involved in the process are divided into three general categories: loss of lithium inventory (LLI), loss of active material and impedance increase [3]. Concretely, such mechanisms can be assumed to include the following: solid electrolyte interphase (SEI) formation, graphitic anode exfoliation and cracking, dendrite growth, cathode disordering, metal dissolution, change in porosity and current collector corrosion [19,20]. Regarding the operational effects produced in cells, two effects can be distinguished: Capacity Fade (CF) and Power Fade (PF). CF is the diminution of the ratio between the current capacity and the rated

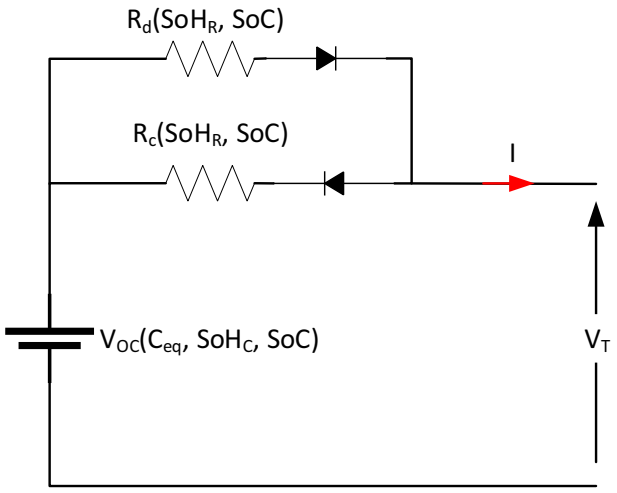

Fig. 4. Internal resistance model.

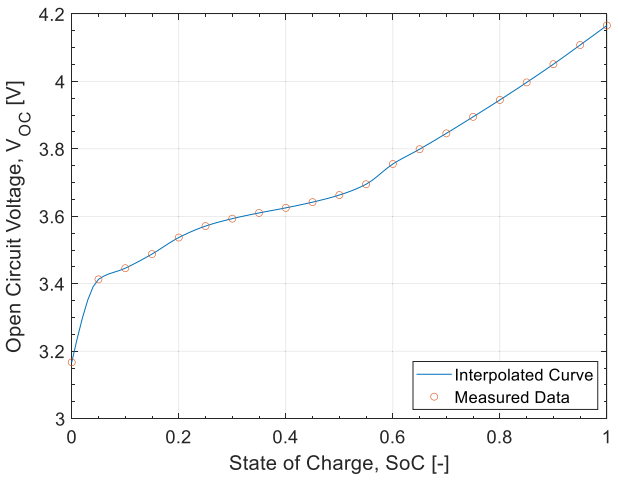

Fig. 5. Characteristics of open-circuit voltage.

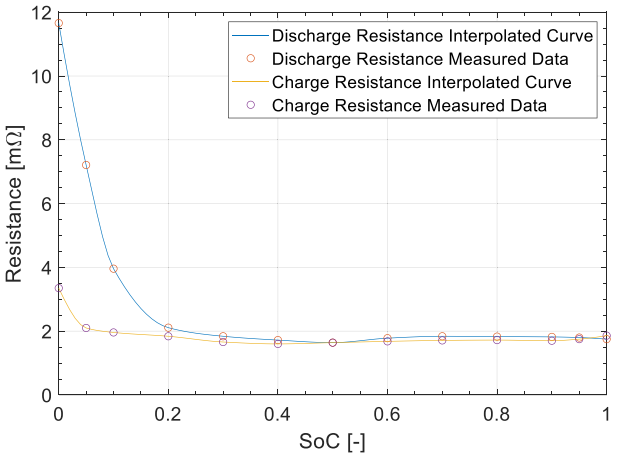

Fig. 6. Characteristics of internal resistance.

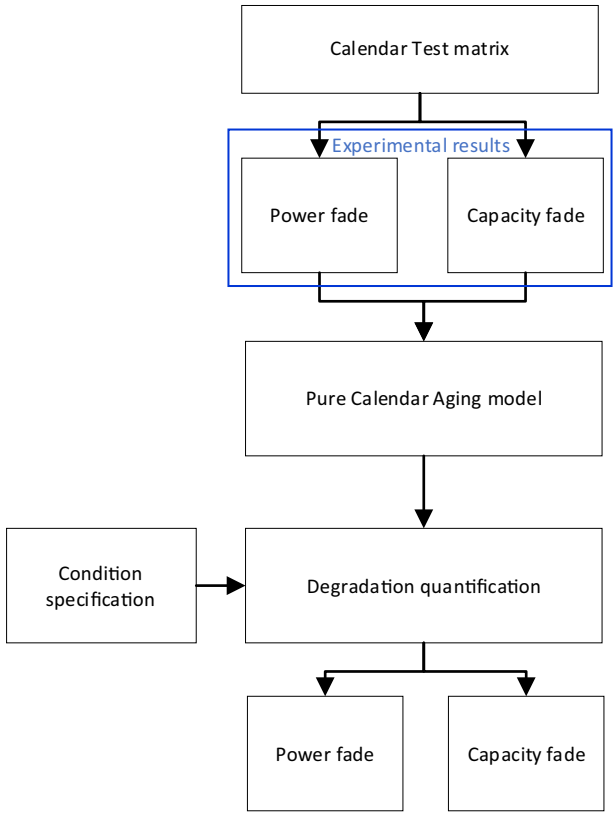

Fig. 7. Overview of the calendar ageing degradation model.

Table 2
Confidence bounds of the calendar ageing model.

Temperature (T)	State of Charge (SoC):	Time (t):
[25–45] °C	[5–90]%	[0–40] weeks
[45–60] °C	[60–90]%	[0–28] weeks

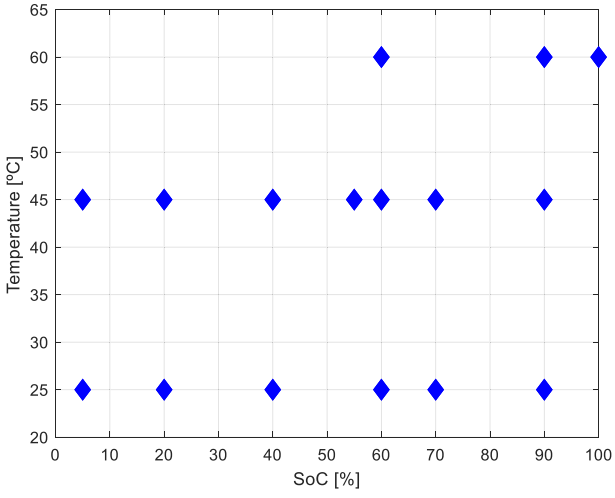

Fig. 8. Calendar ageing test matrix.

capacity and is generally attributed to LLI, whereas PF is the diminution of the ratio between the current maximum power that a cell can deliver and the initial one, caused by an increase of the passivation layer associated with internal resistance [3,21-25]. In the case of EVs, the batteries are usually oversized in terms of power, i.e. they can, generally, deliver more power than what the powertrain components can handle. Consequently, degradation in power terms is not usually considered so critical as CF [26]. However, in the case of BESSs, both CF and PF effects

Table 3
Definition of the compared models.

	Capacity	Resistance	Free parameters
Model 1	$SoH_C = 100 - a_C(SoC,T) \cdot t$	$SoH_R = a_R(SoC,T) \cdot t$	2
Model 2	$SoH_C = 100 - a_C(SoC,T) \cdot \sqrt{t}$	$SoH_R = a_R(SoC,T) \cdot \sqrt{t}$	2
Model 3	$SoH_C = 100 - a_C(SoC,T) \cdot t^{0.75}$	$SoH_R = a_R(SoC,T) \cdot t^{0.75}$	2
Model 4	$SoH_C = 100 - a_C(SoC,T) \cdot t^{b_{(T)}}$	$SoH_R = a_R(SoC,T) \cdot t^{b_{(T)}}$	3

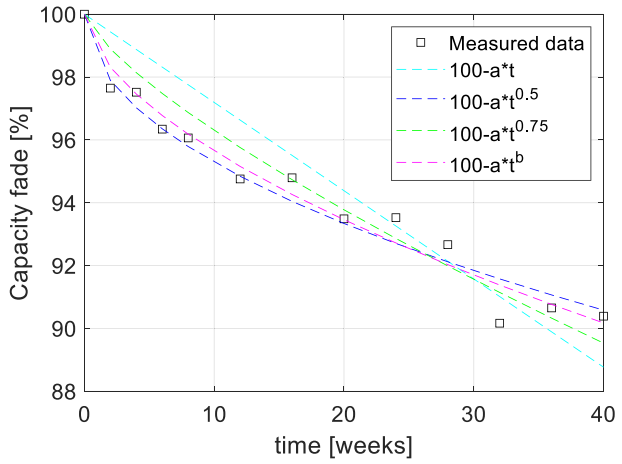

Fig. 9. Different models fittings for 45 °C and 55 % SoC storing calendar capacity fade data.

have to be considered in BESS operation limits definition when designing it, since power and energy conditions have to be met in biddings. In this sense, every demanded services provision must be within BESS operational limits.

Electric energy storage systems degradation models are gaining popularity in academia, as many developments depend on them. Some examples that demonstrate their utility are EVs and BESSs providing ancillary services and contributing to grid stability. Therefore, studies on battery SoH estimation and modeling are encouraged.

Degradation models are usually classified as electrochemical, analytical, electrical and stochastic models. Electrochemical models try to describe ageing using equations based on electrochemical principles [27–32]. Although these models are highly detailed, they usually require a large amount of data extracted from ex-situ techniques (i.e. techniques that cannot be performed in real-time) and need large computation resources. In order to deal with these disadvantages, only main degradation mechanisms are usually considered while others are neglected [33]; this was done in [34] where the authors constructed a degradation model by only considering cathodic degradation mechanisms.

Stochastic models describe ageing with mathematical expressions by taking into consideration probabilistic transitions from previous steps; usually, Markov chains are used to express this evolution. This approach can be particularly accurate in terms of predicting EoL parameters in real-time applications; however, their usages must be carefully evaluated since they do not take into account the physical aspects associated with battery operations.

Analytical models aim to correlate CF and PF with a combination of stress factors (i.e. temperature, SoC and time in the case of calendar ageing). They rely on the data from experimental trials and can decouple degradation in calendar and cycle ageing or compute them as a whole. In this context, some of them propose equations based on the purely best data fitting method (empirical models), while others seek to relate the observed trend with a physical meaning (semi-empirical models). They can deal with ageing in comparison with the equivalent situation (e.g. full cycles to failure) with empirical models or semi-empirical models. The equivalent situation method is the simplest approach where ageing is considered as proportional in every moment, empirical models perform mathematical expressions derived from experimental data fitting and semi-empirical models are based on the physical description of analytical equations. As evident, they also need large testing data, but their execution time is much lower and they can be implemented in battery management systems (BMSs).

Several studies have been conducted in this area. In [35], the authors performed a calendar ageing empirical model of 15 Ah lithium-iron-phosphate (LFP) cells. They modelled CF, but PF was neglected in this study. The same drawback was found in [36]. In [37], however, PF was analysed and CF was neglected in a nickel-cobalt-aluminium (NCA) cell; only high SoC levels were analysed. In [24], authors got an ageing model based on experimental tests, for a wide temperature range (0–60 °C) and SoC range (0–100 %) with up to 2.2 % and 6.9 % of error in CF and PF, respectively. However, the cell that was analysed was a 3 Ah cell, i.e. one with a relatively low capacity for EV applications.

The literature review revealed several works that indicated that calendar ageing CF follows a nonlinear law with time, more concretely, a power law. In this sense, most studies suggested a function proportional to $t^{1/2}$ given by the SEI growth [24,38–44] with an error of 1.0 % to 2.2 % in CF and up to 6.9 % in PF; however, other studies suggested $t^{0.75}$ [45,46] with an error up to 1.1 % in CF or even a linear relationship.

Electrical models update circuital parameters of a previously defined

Table 4
Correlation values (R^2) obtained for data normalisation under calendar ageing for capacity and resistance in every model.

T	SoC	Model 1		Model 2		Model 3		Model 4	
		Cap	R	Cap	R	Cap	R	Cap	R
25 °C	5 %	0.4638	1	0.3823	1	0.432	1	0.3698	1
	40 %	0.8545	1	0.7615	1	0.8457	1	0.7312	1
	60 %	0.7448	1	0.9522	1	0.8905	1	0.9458	1
	70 %	0.699	1	0.969	1	0.8779	1	0.9674	1
	90 %	0.3909	−0.0017	0.929	0.0905	0.6956	0.0474	0.9556	0.1117
45 °C	5 %	0.9693	0.6373	0.8319	0.5353	0.9299	0.6156	0.8735	0.5312
	40 %	0.9375	0.7899	0.9444	0.6878	0.9873	0.7775	0.9745	0.6829
	55 %	0.9041	0.8404	0.9477	0.7918	0.9708	0.8602	0.9707	0.7872
	60 %	0.8699	0.749	0.9551	0.8586	0.9572	0.8485	0.971	0.8564
	70 %	0.8117	0.5008	0.9627	0.85	0.931	0.7144	0.967	0.852
	90 %	0.6934	−0.5455	0.968	0.6066	0.8735	0.0795	0.9507	0.6201
60 °C	60 %	0.8237	0.9602	0.981	0.8091	0.9496	0.9249	0.9596	0.8715
	90 %	0.8013	0.9906	0.9953	0.8742	0.9452	0.976	0.9786	0.933
	100 %	0.4425	0.7959	0.9478	0.9478	0.7411	0.921	0.9759	0.9535
Average R^2		0.7649	0.8186	0.9081	0.8255	0.8710	0.8289	0.9135	0.8351

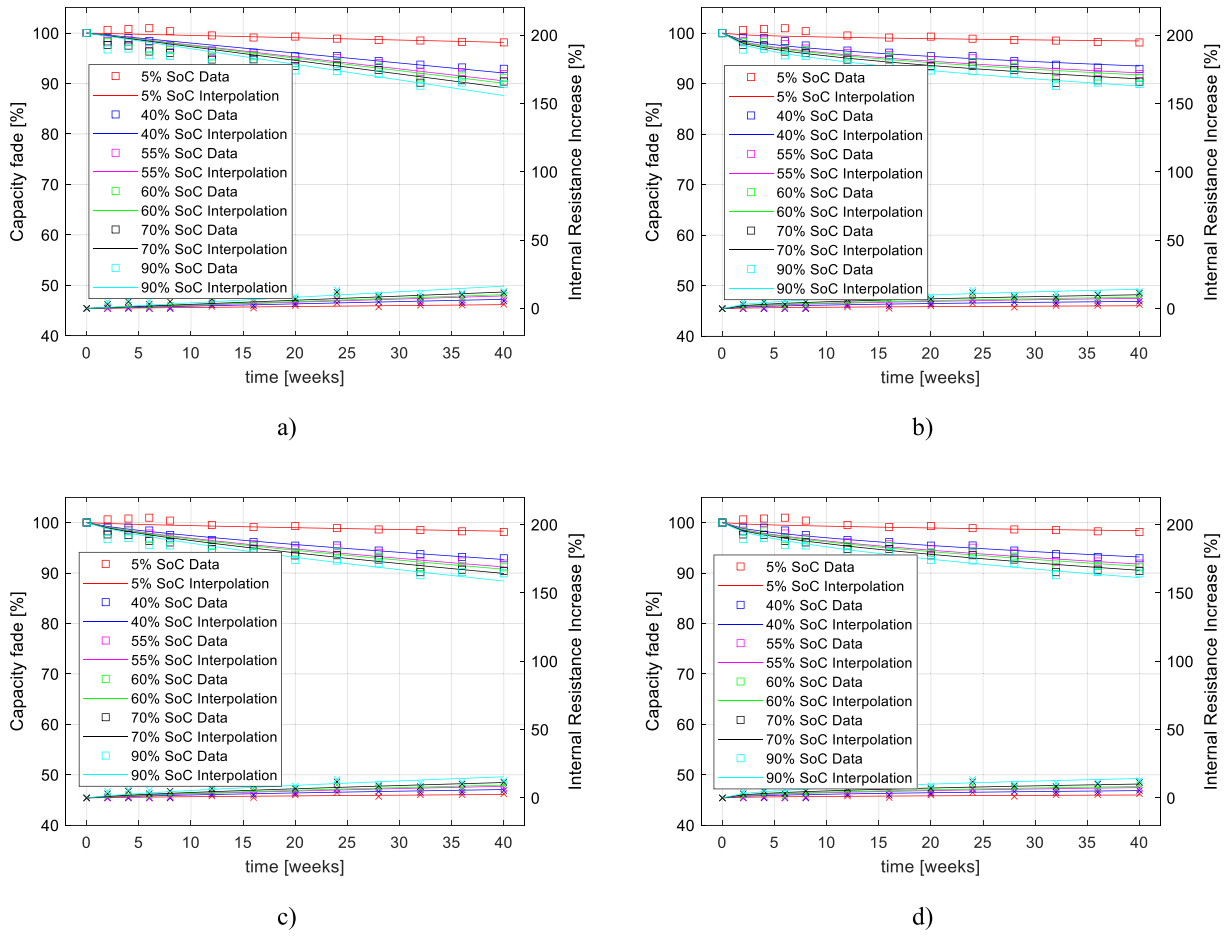

Fig. 10. Calendar ageing under 45 °C temperature fitted with a) Model 1, b) Model 2, c) Model 3, and d) Model 4.

electrical model according to the same stress factors as in analytical models in order to reproduce the terminal voltage. Their accuracy and execution times are dependent on the number of elements in the circuit. Most works focused on analysing the internal resistance evolution using the internal resistance model [47–49], while other works [50,51] used Thevenin models for dynamical simulations in nickel-manganese-cobalt (NMC) or NCA cells and account for CF as well.

In this context, experimental studies on degradation usually considered only a few storage SoCs (or storage voltages) and temperatures; therefore, a general model is needed to obtain results for those conditions that have not been explicitly tested. The model developed in this paper contributed to the literature in the following ways: 1. A relatively fast and high accuracy model was developed; 2. It comprised a wide range of SoC and temperature, which were strongly related to EV and BESS operation; 3. A comparison of the most used model was performed.

Fig. 1 shows the model that was developed, which is compounded by two linked submodels. The first one of them is a semi-empirical submodel of degradation that estimates the degradation of the battery by calendar ageing at the determined conditions, performing several interpolations over the experimental results data set. All the important factors were considered, namely SoC, storing time and temperature with a root-mean-square error (RMSE) of 0.8 % in CF, and a low execution time was maintained. Then, the SoH data was used to upgrade the parameters of the second submodel – an electrical submodel – to calculate the terminal voltage at every storing moment.

This paper is structured as follows: Section 2 shows the studied cell data and the electrical model applied. Section 3 describes the modeling techniques used to develop the battery degradation model, and section 4 describes the degradation model that was developed. Finally, the discussion and conclusions are presented in Section 5.

2. Studied cell data – electrical model

Fig. 2 shows the cell selected for study, the commercially available "Pouch" cell LG Chem E63, which was engineered for high-demanding applications and installed in Renault Zoe EVs. This high-capacity lithium-ion cell includes an NMC cathode and a graphite anode. Table 1 presents the data about this cell [52].

The capacity–temperature relationship of a battery follows a nonlinear law [53,54], as it is graphed in Fig. 3 from the technical product specification report of the manufacturer [55]. Temperature acts as a catalyst; the rate of chemical reactions taking place during the charging and discharging processes is favoured by higher temperatures. These higher rates are considered as higher useful capacity by the user.

In Fig. 3, the continuous curve of the modeling was obtained by applying the Hermite Cubic Interpolation Polynomial (PCHIP). Since it relies on an interpolation method, the obtained curve perfectly aligned with the experimental points obtained in trials. This interpolation method was selected for demonstrating great robustness while respecting the monotonicity of the data. In this context, the PCHIP interpolation [56,57] was previously validated in [52].

The electrical model used here is known as an internal resistance model. In this model, only an internal voltage source representing battery voltage at equilibrium conditions and series resistance were considered. The internal voltage source considered was dependent on capacity, which in turn was given by the actual temperature, SoC and SoH. The resistance considered for charging was different from that for

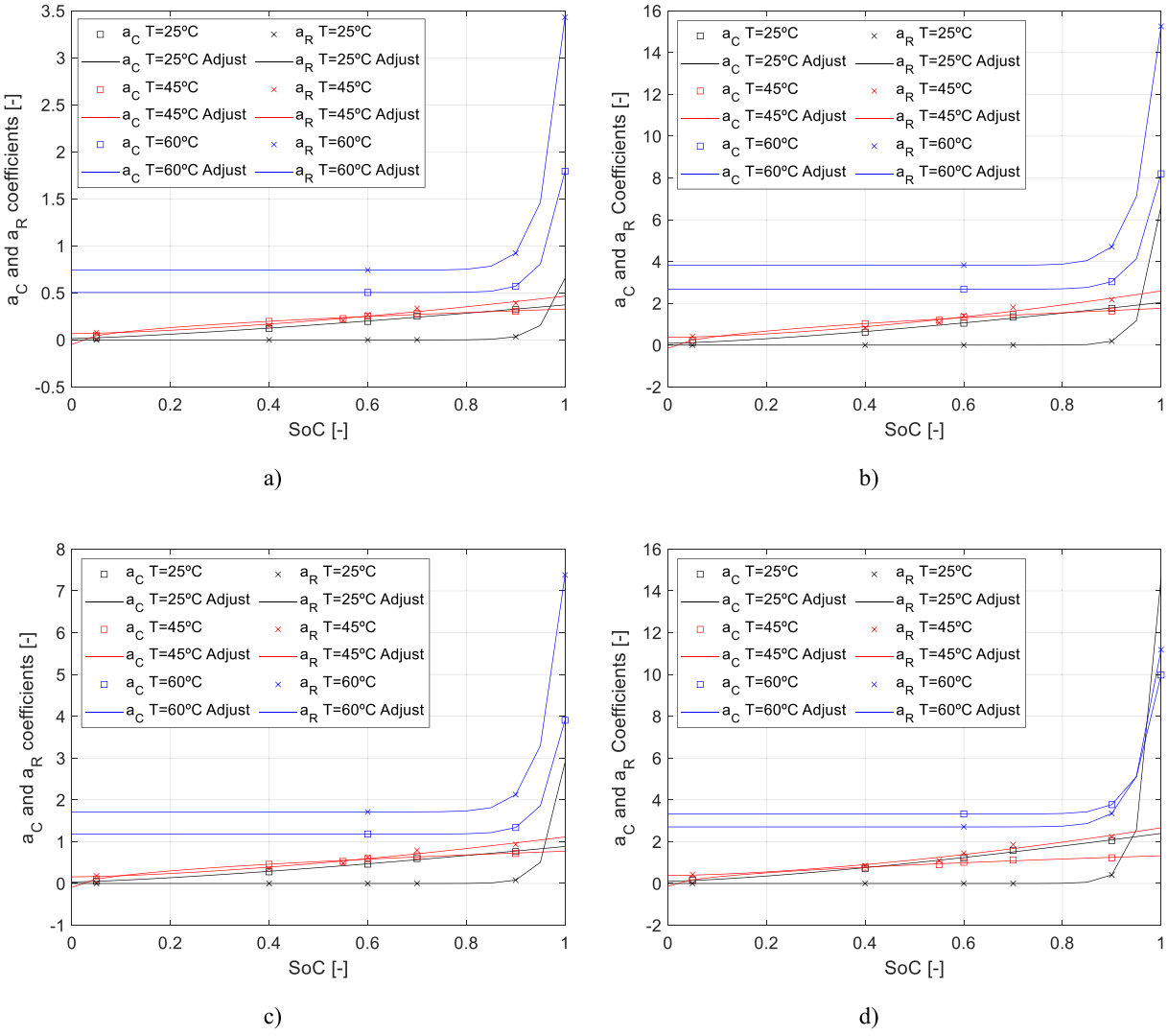

Fig. 11. aC and aR coefficient values in a) Model 1, b) Model 2, c) Model 3 and d) Model 4.

Table 5
Normalised calendar ageing matrix.

SoC [–]	t [weeks]	T
5 %, 20 %, 40 %, 55 %, 60 %, 70 %, 80 %, 90 %, 100 %	0, 2, 4, 6, 8, 12, 16, 20, 24, 28, 32, 36, 40	25 °C 45 °C 60 °C

discharging, but both of them were dependent on the actual SoC and SoH. The capacity state of health (SoH_C), which is related to capacity retention, was also distinguished from the resistance state of health (SoH_R), which is related to the increase in internal resistance, and they were also considered. This differentiation allowed the CF and PF to be decoupled. Fig. 4 shows the internal resistance model considered here.

The expression for calculating the terminal voltage in the internal resistance model is shown in Eq. (1):

$$V_T(t) = V_{OC}(SoC) - R(SoH_R, SoC)\cdot I(t) \quad (1)$$

where $V_T(t)$ is the terminal voltage in each time step, $V_{OC}(SoC)$ is the open-circuit voltage according to SoC, $R(SoH_R, SoC)$ is the internal resistance value according to SoH_R and SoC, and $I(t)$ is the current value in each time step.

Fig. 5 shows the open-circuit voltage (V_{OC}) depending on SoC, which was obtained by applying PCHIP to the available measured data collected from trials.

The open-circuit voltage curve was only experimentally tested at 25 °C; therefore, no open circuit voltage characterization that attended to temperature could be performed.

Fig. 6 shows the internal resistance-SoC characteristic during the processes of charging and discharging; it was obtained by applying PCHIP. The way in which the internal resistance in these cells increases significantly when SoC is low can be observed.

Figs. 5 and 6 show the values corresponding to those of a fresh cell. However, due to degradation by calendar ageing, the capacity decreases, while the internal resistance increases. The evolution rate of these parameters depends on the storage conditions and can be determined using the degradation model explained in this paper. Both submodels were coupled in the following manner: the calendar ageing degradation model determines the actual capacity and internal resistance of the cell after the desired storing time, which then upgrades the parameters of the electrical model.

3. Calendar ageing degradation model

The degradation model that was developed considered battery degradation by calendar ageing in CF and PF terms. For this purpose, a reference matrix was defined, and the ageing given by the desired

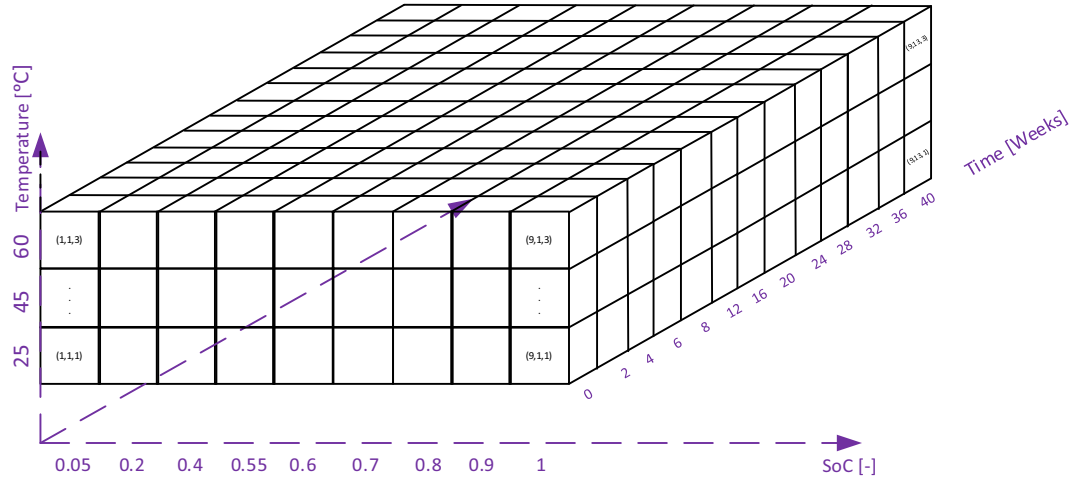

Fig. 12. Structure of the calendar ageing reference matrix.

variables was determined based on the results of some experimental tests. Fig. 7 shows a general overview of the model developed in this paper.

In the process of developing this calendar ageing model, the following statements were assumed:

- Battery degradation can be classified into calendar ageing or cycle ageing. In this paper, it is assumed that these phenomena can be distinguished and decoupled [58], since the model here developed is based on storage experiments all degradation is assumed to be calendar ageing. Cycle ageing during capacity tests is neglected.
- Since this model relies on interpolations, the available data define the highest confidence bounds, which are shown in Table 2. However, it is also possible to use this model to calculate battery degradation out of these confidence bounds.

3.1. Test matrix

The cells under study were tested under 16 different storage conditions in [55], and Fig. 8 specifies the test matrix.

The studied cells were stored at a specified SoC and temperature, and the capacity and internal resistance measurements were taken, generally, in steps over 4 weeks. These measurements were performed in the following manner: the cells were put in a chamber at 25 °C for one hour; then, they were discharged at 32.5 A (constant current), i.e. at C/2C-rate until the undervoltage limit of 2.50 V was reached. Then, the cells were charged at a constant current in two stages: the first at 21.6 A (C/3) and the second at 13 A (C/5) until 4.05 V and 4.20 V were reached, respectively. This discharging–charging process was repeated twice in order to collect average measurements.

3.2. Data treatment and normalisation

Data treatment and normalisation were performed after collecting all of the experimental test results to get a normalised data matrix, i.e. even if the experimental trials were conducted at certain conditions of SoC, temperature and time, the developed model could estimate degradation values using any value of these variables.

For every test conducted, a concrete equation describing degradation was obtained by considering every SoC, t and T based on Eqs. (2) and (3).

$$SoH_C = 100 - a_C(SoC, T)\cdot t^{b_C(T)} \tag{2}$$

$$SoH_R = a_R(SoC, T)\cdot t^{b_R(T)} \tag{3}$$

where SoH is the state of health, a is a prepotential factor, t is the number of weeks and b is a potential factor. SoH_C, SoH_R, a_C, a_R, b_C, and b_R are distinguished for CF and PF, respectively.

The great relevance of the precision ensured while modeling the degradation in the tested cells by fitting equations should be noted since all interpolations will rely on this precision. Better fittings will always lead to a better result independent of the point of interest.

Concretely and based on Eqs. (11) and (12), four models were tested in search of the best fitting. These models were also selected according to such models available in the literature. Among these four models, different time depending rates were considered. Table 3 presents the model definitions that were considered, while Fig. 9 shows the fittings of these models to an experimentally taken data set. As can be observed, all of them had a general good fitting, although certain considerations were there, which are explained later on.

The capacity and internal resistance of a cell at actual conditions were determined by Eqs. (4) and (5).

$$Cap(SoH_C) = Cap_N\cdot SoH_C \tag{4}$$

$$R(SoC, SoH_R) = R(SoC)\cdot(1 + SoH_R) \tag{5}$$

where $Cap(SoH_C)$ is the actual capacity at current on SoH, Cap_N is the nominal capacity, $R(SoH_C, SoH_R)$ is the actual resistance at current SoC and SoH and $R(SoC)$ is the resistance at current SoC in a fresh cell.

For every data set (for every temperature and SoC), a nonlinear regression fit was calculated while taking the following into consideration:

- All data sets were fitted to every model based on Eqs. (2) or (3), and they are specified in Table 3.
- All data sets regarding the same temperature were normalised using a nonlinear square regressions algorithm of multiple data sets, and the b potential factor was set to a constant along T to obtain non-crossed curves. In Models 1–3, the b factor was 1, 0.5 and 0.75, respectively, while in Model 4, it was free to fit.

Consequently, the a prepotential factor varied along the storing SoC and T, while the b potential factor varied only along the storing T. Table 4 presents R^2 correlating factor values for every data set and model definition as well as an average measure calculated as RMS for every model.

Fig. 10 shows the results for 45 °C, indicating the discrete points

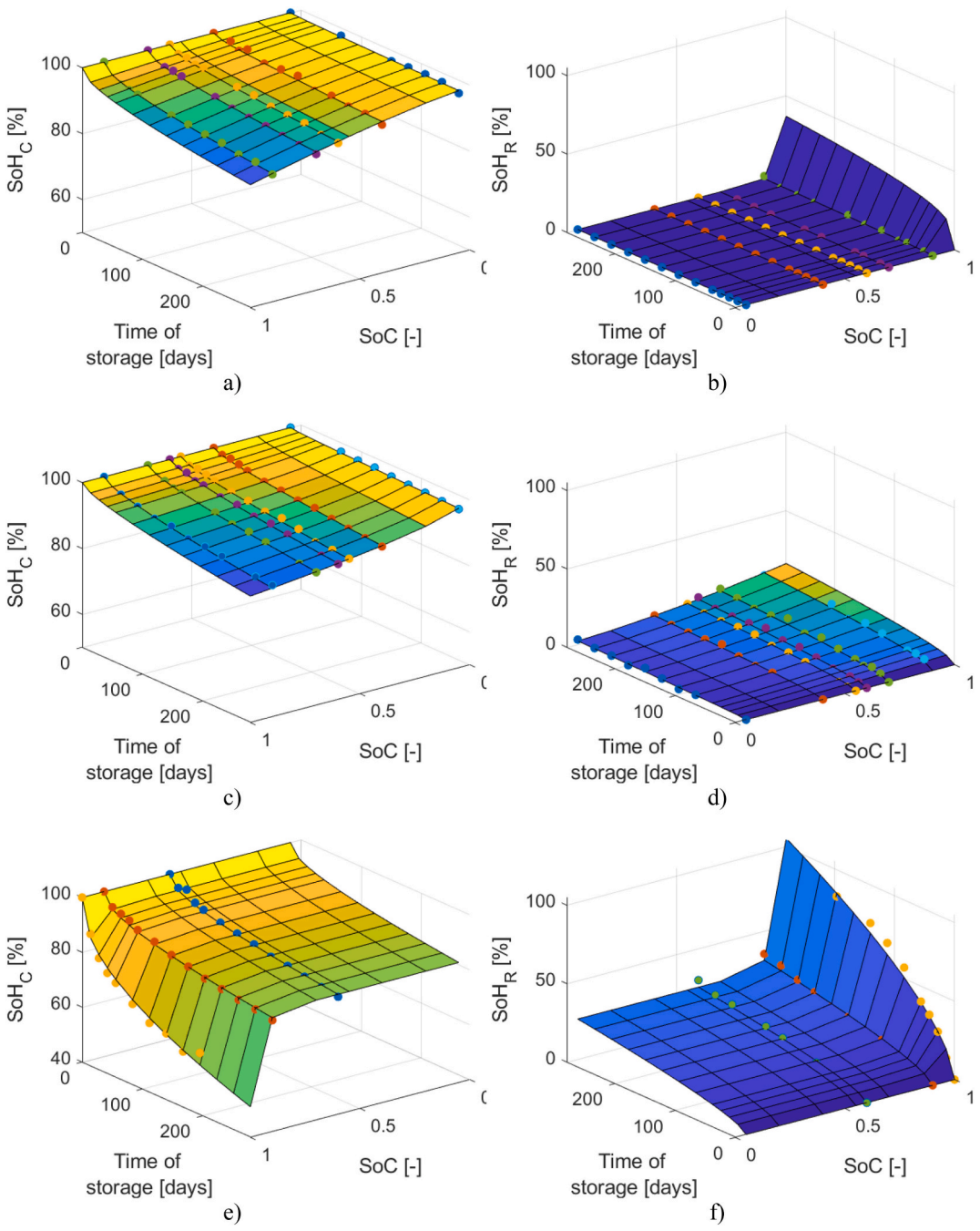

Fig. 13. a) CF for 25 °C, b) PF for 25 °C, c) CF for 45 °C, d) PF for 45 °C, e) CF for 60 °C and f) PF for 60 °C.

obtained from the experimental tests and the continuous curves obtained by applying Models 1–4. Upper and lower boundaries were applied to the models in order to omit capacity data points over 100 % and internal resistance increase data points below 0 %, as they were either considered as transient stages or not as a tendency. As evident from Table 4 and Fig. 10, Model 4 showed the greatest fit, improving the accuracy by, on average, 0.54 % in CF and 0.96 % in PF, compared to the commonly used Model 2. Additionally, Model 1 seemed to be a better approximation when SoCs and temperature were low, but it got worse as the SoC increased. However, for medium SoC values, Model 3 displayed better behaviour. This showed that battery degradation in these cells could be represented by a linear behaviour at low SoCs and temperatures, and this behaviour became nonlinear as the SoC rises or when the temperature is relatively high. Therefore, Model 4 was chosen as the best fit and was applied thereafter.

After performing an analysis of the a parameter values, it was concluded that the a parameter follows the potential law presented in Eqs. (6) and (7).

$$a_C = d_C \cdot SoC^{e_C} + f_C \tag{6}$$

$$a_R = d_R \cdot SoC^{e_R} + f_R \tag{7}$$

Fig. 11 shows a parameter factor values along SoC for all the models that were studied. R^2 correlation values for this adjust were above 0.9937 in capacity and 0.9638 in resistance (for Model 4).

This adjustment was applied to obtain the value of the a_C pre-potential factor for every value of SoC at 25 °C, 45 °C and 60 °C. By combining these adjustments with Model 4, the calendar ageing modeling expressions were obtained. After sorting them, a reference

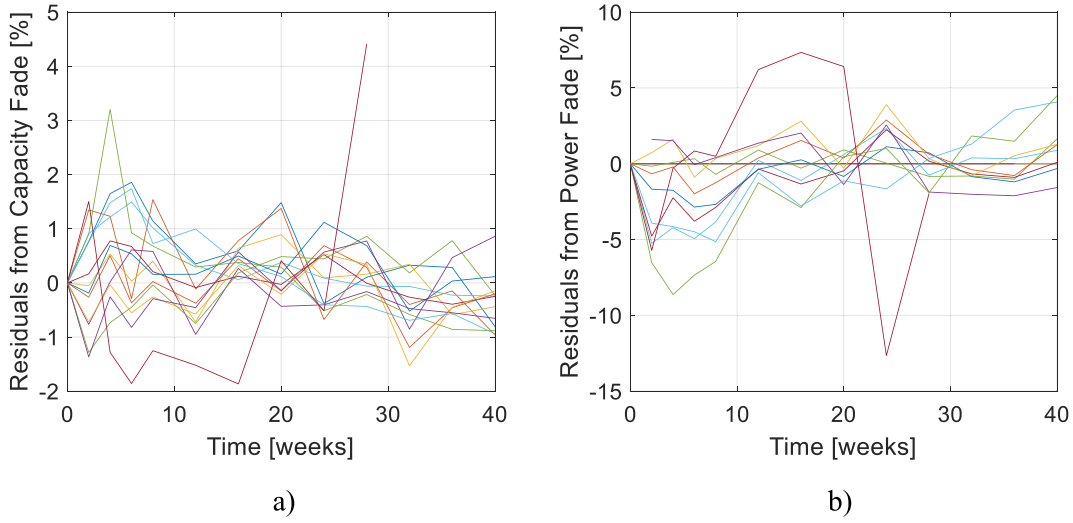

Fig. 14. Residual plots for capacity fade and power fade.

normalised matrix was obtained, and Table 5 shows the structure of this matrix.

4. General model development

Based on the normalised calendar ageing and to calculate every storing condition, the model calculated the PCHIP interpolating parameters that fit the available data better. Therefore, the model considered a dynamic interpolating algorithm that recalculated every PCHIP parameter value depending on the storing conditions.

The calendar ageing interpolation was executed in 3 variables or dimensions, namely storing SoC, time and temperature**.** The determination of degradation at the desired SoC and temperature was calculated based on PCHIP, while the time of storing, *t*, reconstructed the equation for model 4 from Table 3. Fig. 12 shows the resulting 3D reference matrix structure.

The developed model in Matlab R2021a offered a low computational demand and high speed, needing as much as 0.57 s to calculate both CF and PF for the required conditions on an intel i7 2.80 GHz processor. This highest resource-demanding scenario matched the case where all variables needed to be interpolated. Fig. 13 indicates the validation of the CF and PF model results.

The same process was performed with the three other models, requiring the execution time of 0.33 s, 0.27 s and 0.31 s for Model 1, Model 2 and Model 3, respectively. In this context, the most accurate model was also the slowest one, requiring an execution time that was approximately double than that in the most commonly used model (i.e. Model 2), but it was still reasonable.

As expected, it was observed that greater SoC was linked with a greater degradation of the cell, both in CF and PF. Additionally, regarding temperature, it was found that there was no great significance when the temperature was maintained with the range of 25 °C–45 °C range; however, it was a major factor when it was over 45 °C. High temperature and high SoC were found to be the most harmful state for these cells.

Residuals or relative errors were also calculated for every condition that was tested, and they were calculated as follows:

$$e_{iC} = \frac{SoH_{i,C\ meas} - SoH_{i,C\ estim}}{SoH_{i,C\ meas}} \tag{8}$$

$$e_{i,R} = \frac{SoH_{i,R\ meas} - SoH_{i,R\ estim}}{SoH_{i,R\ meas}} \tag{9}$$

Fig. 14 plots all residuals for CF and PF.

As seen in Fig. 14, since most of the points were over zero, the developed model tended to underestimate the capacity of the cell or SoH_C, which meant that this model could be regarded as conservative. A conservative model is advantageous when it is used in EV or BESS applications since the estimated SoH is below the real one, thereby reducing the probability of not fulfilling the needs of the application. In PF, however, in the initial stages of storing, the model tended to overestimate SoH_R and started to underestimate it as time went by. While simulating CF, the maximum error was reported to be 4.4 % when SoC = 1, t = 28 weeks and T = 60 °C, while the average RMSE was 0.8 %. Regarding PF simulation, the maximum error obtained was 12.7 % when SoC = 1, t = 24 weeks and T = 60 °C, while the average RMSE was 2.3 %.

5. Discussion and conclusions

Calendar ageing is an important degradation factor that must be considered in every work related to EVs and BESSs. In this context, this paper presented a simple but accurate electrical and degradation model for an NMC cell battery that is already being used in a commercial EV. It was assumed that 20 % of the degraded cells were not valid for electromobility, and a second life for these cells needed to be found. Their use in stationary applications such as BESS is gaining interest; therefore, degradation models concerning both applications are needed.

Four models were compared in order to identify the most accurate one. In this sense, was determined that the commonly used model with 0.5 degradation rate (Model 2) has good accuracy, especially considering its operation speed; however, it can be improved by determining a custom degradation rate. Although its operation speed is lowered to, approximately, the half in comparison with Model 2, it is still a reasonable speed and is compatible with real-time operations.

The developed model represented the degradation by calendar ageing with an RMSE of 0.8 % in CF and 2.3 % in PF under a wide range of SoCs and temperatures for the desired storing time. It was observed that the temperature and SoCs above certain values have the highest impact on battery degradation and keeping cells at a relatively medium or low SoC and temperature can be highly beneficial.

CRediT authorship contribution statement

Gaizka Saldaña: Conceptualization, Methodology, Investigation, Formal analysis, Writing – original draft. **José Ignacio San Martín:** Supervision, Project administration, Funding acquisition. **Inmaculada Zamora:** Supervision, Project administration, Funding acquisition. **Francisco Javier Asensio:** Conceptualization, Writing – review &

editing. **Oier Oñederra:** Writing – review & editing, Visualization. **Mikel González-Pérez:** Investigation, Visualization.

Declaration of competing interest

The authors declare that they have no known competing financial interests or personal relationships that could have appeared to influence the work reported in this paper.

Data availability

Data used is referenced in references section

Acknowledgements

The authors thank the Basque Government (project PIBA_2019_1_0098, KK-2022/00100 and GISEL research group IT1522-22) and the University of the Basque Country UPV/EHU (project COLAB19 and PES16/31) for their support.

Appendix A. Appendix

Table A
Subscripts.

C	Capacity
i	Data number
R	Resistance
meas	Measured
estim	Estimated
T	Terminal
oc	Open circuit

Table B
Notations.

V	Voltage
i	Data number
R	Resistance
meas	Measured
estim	Estimated
I	Current
a	Prepotential factor
b	Potential factor
cap	Capacity
d	Prepotential factor for a
e	Potential factor for a
f	Offset factor

References

[1] M. Rahman, M. Rahman, X. Wang, X. Wang, C. Wen, C. Wen, in: A Review of High Energy Density Lithium–air Battery Technology 44, 2014, pp. 5–22, https://doi.org/10.1007/s10800-013-0620-8.
[2] A.W. Thompson, in: Economic Implications of Lithium Ion Battery Degradation for Vehicle-to-Grid (V2X) Services 396, 2018, pp. 691–709, https://doi.org/10.1016/j.jpowsour.2018.06.053.
[3] M. Dubarry, N. Qin, P. Brooker, in: Calendar Aging of Commercial Li-ion Cells of Different Chemistries – A Review 9, 2018, pp. 106–113, https://doi.org/10.1016/j.coelec.2018.05.023.
[4] S.L. Hahn, M. Storch, R. Swaminathan, B. Obry, J. Bandlow, K.P. Birke, in: Quantitative Validation of Calendar Aging Models for Lithium-ion Batteries 400, 2018, pp. 402–414, https://doi.org/10.1016/j.jpowsour.2018.08.019.
[5] J. García-Villalobos, I. Zamora, J. San Martín, F. Asensio, V. Aperribay, in: Plug-in Electric Vehicles in Electric Distribution Networks: A Review of Smart Charging Approaches 38, 2014, pp. 717–731, https://doi.org/10.1016/j.rser.2014.07.040.
[6] F. Eckermann, M. Kahlert, C. Wietfeld, in: Performance Analysis of C-V2X Mode 4 Communication Introducing an Open-source C-V2X Simulator, IEEE, 2019, pp. 1–5, https://doi.org/10.1109/VTCFall.2019.8891534.
[7] G. Saldaña, J.I.San Martin, I. Zamora, F.J. Asensio, O. Oñederra, in: Electric Vehicle into the Grid: Charging Methodologies Aimed at Providing Ancillary Services Considering Battery Degradation 12, 2019, p. 2443, https://doi.org/10.3390/en12122443.
[8] M. Dubarry, A. Devie, K. Stein, M. Tun, M. Matsuura, R. Rocheleau, in: Battery Energy Storage System Battery Durability and Reliability Under Electric Utility Grid Operations: Analysis of 3 Years of Real Usage 338, 2017, pp. 65–73, https://doi.org/10.1016/j.jpowsour.2016.11.034.
[9] L. Zhou, Y. Zhang, X. Lin, C. Li, Z. Cai, P. Yang, in: Optimal Sizing of PV and BESS for a Smart Household Considering Different Price Mechanisms 6, 2018, pp. 41050–41059, https://doi.org/10.1109/ACCESS.2018.2845900.
[10] M. Förstl, D. Azuatalam, A. Chapman, G. Verbič, A. Jossen, H. Hesse, in: Assessment of Residential Battery Storage Systems and Operation Strategies Considering Battery Aging 44, 2019, pp. 718–731, https://doi.org/10.1002/er.4770.
[11] C. Di Bari A. Lecocq G. Marlair B. Truchot M. Mazzaro M.L. Mele P. Russo , Recent Safety Focused Overall Analysis, Testing and Accident Reviews Towards Safer e-mobility and Energy Storage, (n.d.).
[12] C. Geisbauer, K. Wöhrl, C. Mittmann, H.-G. Schweiger, in: Review-Review of Safety Aspects of Calendar Aged Lithium Ion Batteries 167, 2020, p. 90523, https://doi.org/10.1149/1945-7111/ab89bf.
[13] A.R. Bais, D.G. Subhedar, S. Panchal, in: Critical Thickness of Nano-enhanced RT-42 Paraffin Based Battery Thermal Management System for Electric Vehicles: A Numerical Study 52, 2022, p. 104757, https://doi.org/10.1016/j.est.2022.104757.
[14] X. Li, J. Zhao, J. Duan, S. Panchal, J. Yuan, R. Fraser, M. Fowler, M. Chen, in: Simulation of Cooling Plate Effect on a Battery Module With Different Channel Arrangement 49, 2022, p. 104113, https://doi.org/10.1016/j.est.2022.104113.
[15] Z. Zhao, S. Panchal, P. Kollmeyer, A. Emadi, O. Gross, D. Dronzkowski, V. Mahajan, L. David, 3D FEA Thermal Modeling with Experimentally Measured Loss Gradient of Large Format Ultra-Fast Charging Battery Module Used for EVs, 2022, https://doi.org/10.4271/2022-01-0711.
[16] Y. Liang, A. Emadi, O. Gross, C. Vidal, M. Canova, S. Panchal, P. Kollmeyer, M. Naguib, F. Khanum, A Comparative Study between Physics, Electrical and Data Driven Lithium-Ion Battery Voltage Modeling Approaches, 2022, https://doi.org/10.4271/2022-01-0700.
[17] T.T.D. Nguyen, S. Abada, A. Lecocq, J. Bernard, M. Petit, G. Marlair, S. Grugeon, S. Laruelle, in: Understanding the Thermal Runaway of Ni-Rich Lithium-Ion Batteries 10, 2019, p. 79, https://doi.org/10.3390/wevj10040079.
[18] S. Abada, M. Petit, A. Lecocq, G. Marlair, V. Sauvant-Moynot, F. Huet, in: Combined Experimental and Modeling Approaches of the Thermal Runaway of Fresh and Aged Lithium-ion Batteries 399, 2018, pp. 264–273, https://doi.org/10.1016/j.jpowsour.2018.07.094.

[19] S.-P. Kim, A.C.T. van Duin, V.B. Shenoy, in: Effect of Electrolytes on the Structure and Evolution of the Solid Electrolyte Interphase (SEI) in Li-ion Batteries: A Molecular Dynamics Study 196, 2011, pp. 8590–8597, https://doi.org/10.1016/j.jpowsour.2011.05.061.
[20] N. Dupré, J.-F. Martin, J. Oliveri, P. Soudan, A. Yamada, R. Kanno, D. Guyomard, in: Relationship Between Surface Chemistry and Electrochemical Behavior of LiNi1/2Mn1/2O2 Positive Electrode in a Lithium-ion Battery 196, 2011, pp. 4791–4800, https://doi.org/10.1016/j.jpowsour.2010.07.049.
[21] A. Eddahech, O. Briat, J.-M. Vinassa, in: Performance Comparison of Four Lithium–ion Battery Technologies Under Calendar Aging 84, 2015, pp. 542–550, https://doi.org/10.1016/j.energy.2015.03.019.
[22] P. Keil, S.F. Schuster, J. Wilhelm, J. Travi, A. Hauser, R.C. Karl, A. Jossen, in: Calendar Aging of Lithium-Ion Batteries 163, 2016, pp. A1872–A1880, https://doi.org/10.1149/2.0411609jes.
[23] D. Li, D.L. Danilov, J. Xie, L. Raijmakers, L. Gao, Y. Yang, P.H. Notten, Degradation mechanisms of C6/LiFePO4 batteries: experimental analyses of calendar, Aging 190 (2016) 1124–1133, https://doi.org/10.1016/j.electacta.2015.12.161.
[24] M. Naumann, M. Schimpe, P. Keil, H.C. Hesse, A. Jossen, in: Analysis and Modeling of Calendar Aging of a Commercial LiFePO4/graphite Cell 17, 2018, pp. 153–169, https://doi.org/10.1016/j.est.2018.01.019.
[25] T. Lu, Y. Luo, Y. Zhang, W. Luo, L. Yan, J. Xie, in: Degradation Analysis of Commercial Lithium-Ion Battery in Long-Term Storage 164, 2017, pp. A775–A784, https://doi.org/10.1149/2.1321704jes.
[26] Junyi Shen, S. Dusmez, A. Khaligh, in: Optimization of Sizing and Battery Cycle Life in Battery/Ultracapacitor Hybrid Energy Storage Systems for Electric Vehicle Applications 10, 2014, pp. 2112–2121, https://doi.org/10.1109/TII.2014.2334233.
[27] R. Xiong, L. Li, Z. Li, Q. Yu, H. Mu, in: An Electrochemical Model Based Degradation State Identification Method of Lithium-ion Battery for All-climate Electric Vehicles Application 219, 2018, pp. 264–275, https://doi.org/10.1016/j.apenergy.2018.03.053.
[28] S. Tippmann, D. Walper, L. Balboa, B. Spier, W.G. Bessler, in: Low-temperature Charging of Lithium-ion Cells Part I: Electrochemical Modeling and Experimental Investigation of Degradation Behavior 252, 2014, pp. 305–316, https://doi.org/10.1016/j.jpowsour.2013.12.022.
[29] L. Zheng, L. Zhang, J. Zhu, G. Wang, J. Jiang, in: Co-estimation of State-of-charge, Capacity and Resistance for Lithium-ion Batteries Based on a High-fidelity Electrochemical Model 180, 2016, pp. 424–434, https://doi.org/10.1016/j.apenergy.2016.08.016.
[30] M. Huang M. Kumar C. Yang A. Soderlund , Aging Estimation of Lithium-ion Battery Cell using an Electrochemical Model-Based Extended Kalman Filter, n.d. doi:10.2514/6.2019-0785.
[31] X. Zhang, Y. Gao, B. Guo, C. Zhu, X. Zhou, L. Wang, J. Cao, in: A Novel Quantitative Electrochemical Aging Model Considering Side Reactions for Lithium-ion Batteries 343, 2020, p. 136070, https://doi.org/10.1016/j.electacta.2020.136070.
[32] B. Stiaszny, J.C. Ziegler, E.E. Krauß, M. Zhang, J.P. Schmidt, E. Ivers-Tiffée, in: Electrochemical Characterization and Post-mortem Analysis of Aged LiMn2O4–NMC/graphite Lithium Ion Batteries Part II: Calendar Aging 258, 2014, pp. 61–75, https://doi.org/10.1016/j.jpowsour.2014.02.019.
[33] K. Liu, X. Hu, M. Lucu, W.D. Widanage, T. Ashwin, in: An Evaluation Study of Different Modelling Techniques for Calendar Ageing Prediction of Lithium-ion Batteries 131, 2020, p. 110017, https://doi.org/10.1016/j.rser.2020.110017.
[34] A.P. Schmidt, M. Bitzer, Á.W. Imre, L. Guzzella, in: Model-based Distinction and Quantification of Capacity Loss and Rate Capability Fade in Li-ion Batteries 195, 2010, pp. 7634–7638, https://doi.org/10.1016/j.jpowsour.2010.06.011.
[35] S. Grolleau, A. Delaille, H. Gualous, P. Gyan, R. Revel, J. Bernard, E. Redondo-Iglesias, J. Peter, in: Calendar Aging of Commercial Graphite/LiFePO4 Cell – Predicting Capacity Fade Under Time Dependent Storage Conditions 255, 2014, pp. 450–458, https://doi.org/10.1016/j.jpowsour.2013.11.098.
[36] D. Galatro, C.D. Silva, D.A. Romero, O. Trescases, C.H. Amon, in: Challenges in Data-based Degradation Models for Lithium-ion Batteries 44, 2020, pp. 3954–3975, https://doi.org/10.1002/er.5196.
[37] E. Thomas, H. Case, D. Doughty, R. Jungst, G. Nagasubramanian, E. Roth, in: Accelerated Power Degradation of Li-ion Cells 124, 2003, pp. 254–260, https://doi.org/10.1016/S0378-7753(03)00729-8.
[38] T. Matsushima, in: Deterioration Estimation of Lithium-ion Cells in Direct Current Power Supply Systems and Characteristics of 400-Ah Lithium-ion Cells 189, 2009, pp. 847–854, https://doi.org/10.1016/j.jpowsour.2008.08.023.
[39] E. Sarasketa-Zabala, I. Gandiaga, I. Villarreal, L. Rodriguez-Martinez, in: Calendar Ageing Analysis of a LiFePO4/graphite Cell With Dynamic Model Validations: Towards Realistic Lifetime Predictions 272, 2014, pp. 45–57, https://doi.org/10.1016/j.jpowsour.2014.08.051.
[40] Y. Liu, K. Xie, Y. Pan, H. Wang, Y. Li, C. Zheng, in: Simplified Modeling and Parameter Estimation to Predict Calendar Life of Li-ion Batteries 320, 2018, pp. 126–131, https://doi.org/10.1016/j.ssi.2018.02.038.
[41] I. Bloom, L.K. Walker, J.K. Basco, D.P. Abraham, J.P. Christophersen, C.D. Ho, Differential voltage analyses of high-power lithium-ion cells. 4, in: Cells Containing NMC 195, 2010, pp. 877–882, https://doi.org/10.1016/j.jpowsour.2009.08.019.
[42] S. Käbitz, J.B. Gerschler, M. Ecker, Y. Yurdagel, B. Emmermacher, D. André, T. Mitsch, D.U. Sauer, in: Cycle and Calendar Life Study of a Graphite|LiNi1/3Mn1/3Co1/3O2 Li-ion High Energy System. Part A: Full Cell Characterization 239, 2013, pp. 572–583, https://doi.org/10.1016/j.jpowsour.2013.03.045.
[43] J. Schmitt, A. Maheshwari, M. Heck, S. Lux, M. Vetter, in: Impedance Change and Capacity Fade of Lithium Nickel Manganese Cobalt Oxide-based Batteries During Calendar Aging 353, 2017, pp. 183–194, https://doi.org/10.1016/j.jpowsour.2017.03.090.
[44] J. Wang, J. Purewal, P. Liu, J. Hicks-Garner, S. Soukazian, E. Sherman, A. Sorenson, L. Vu, H. Tataria, M.W. Verbrugge, in: Degradation of Lithium Ion Batteries Employing Graphite Negatives and Nickel–cobalt–manganese Oxide + Spinel Manganese Oxide Positives: Part 1, Aging Mechanisms and Life Estimation 269, 2014, pp. 937–948, https://doi.org/10.1016/j.jpowsour.2014.07.030.
[45] J. Schmalstieg, S. Käbitz, M. Ecker, D.U. Sauer, in: A Holistic Aging Model for Li(NiMnCo)O2 Based 18650 Lithium-ion Batteries 257, 2014, pp. 325–334, https://doi.org/10.1016/j.jpowsour.2014.02.012.
[46] R. Mathieu, I. Baghdadi, O. Briat, P. Gyan, J.-M. Vinassa, in: D-optimal Design of Experiments Applied to Lithium Battery for Ageing Model Calibration 141, 2017, pp. 2108–2119, https://doi.org/10.1016/j.energy.2017.11.130.
[47] S.B. Vilsen, S.Knudsen Kaer, D. Stroe, in: Predicting Lithium-ion Battery Resistance Degradation Using a Log-Linear Model, IEEE, 2019, pp. 1136–1143, https://doi.org/10.1109/ECCE.2019.8912770.
[48] R. Wright, C. Motloch, J. Belt, J. Christophersen, C. Ho, R. Richardson, I. Bloom, S. Jones, V. Battaglia, G. Henriksen, T. Unkelhaeuser, D. Ingersoll, H. Case, S. Rogers, R. Sutula, in: Calendar- and Cycle-life Studies of Advanced Technology Development Program Generation 1 Lithium-ion Batteries 110, 2002, pp. 445–470, https://doi.org/10.1016/S0378-7753(02)00210-0.
[49] D.-I. Stroe, M. Swierczynski, S.K. Kar, R. Teodorescu, in: A Comprehensive Study on the Degradation of Lithium-ion Batteries During Calendar Ageing: The Internal Resistance Increase, IEEE, 2016, pp. 1–7, https://doi.org/10.1109/ECCE.2016.7854664.
[50] M. Einhorn, V.F. Conte, C. Kral, J. Fleig, R. Permann, in: Parameterization of an Electrical Battery Model for Dynamic System Simulation in Electric Vehicles, IEEE, 2010, pp. 1–7, https://doi.org/10.1109/VPPC.2010.5729127.
[51] B.Y. Liaw, R.G. Jungst, G. Nagasubramanian, H.L. Case, D.H. Doughty, in: Modeling Capacity Fade in Lithium-ion Cells 140, 2005, pp. 157–161, https://doi.org/10.1016/j.jpowsour.2004.08.017.
[52] G. Saldana, J.I.S. Martin, I. Zamora, F.J. Asensio, O. Onederra, M. Gonzalez, in: Empirical Electrical and Degradation Model for Electric Vehicle Batteries 8, 2020, pp. 155576–155589, https://doi.org/10.1109/ACCESS.2020.3019477.
[53] A.A. Hussein, in: Experimental Modeling and Analysis of Lithium-ion Battery Temperature Dependence, IEEE, 2015, pp. 1084–1088, https://doi.org/10.1109/APEC.2015.7104483.
[54] G.R. Molaeimanesh, S.M. Mousavi-Khoshdel, A.B. Nemati, Experimental Analysis of Commercial LiFePO4 Battery Life Span Used in Electric Vehicle Under Extremely Cold and Hot Thermal Conditions, 2020, https://doi.org/10.1007/s10973-020-09272-z.
[55] Rechargeable Lithium Ion Battery E63, LG Chem, Seoul, South Korea, Feb. 2018. Tech. Rep.
[56] P.M. Barker, T.J. McDougall, in: Two Interpolation Methods Using Multiply-Rotated Piecewise Cubic Hermite Interpolating Polynomials 37, 2020, pp. 605–619, https://doi.org/10.1175/JTECH-D-19-0211.1.
[57] F.J. Asensio, J.I.San Martín, I. Zamora, O. Oñederra, in: Model for Optimal Management of the Cooling System of a Fuel Cell-based Combined Heat and Power System for Developing Optimization Control Strategies 211, 2018, pp. 413–430, https://doi.org/10.1016/j.apenergy.2017.11.066.
[58] B. Xu, A. Oudalov, A. Ulbig, G. Andersson, D.S. Kirschen, in: Modeling of Lithium-Ion Battery Degradation for Cell Life Assessment 9, 2018, pp. 1131–1140, https://doi.org/10.1109/TSG.2016.2578950.